

# Mesoscopic lattice Boltzmann modeling of flowing soft systems

Roberto Benzi

*University of Tor Vergata and INFN, via della Ricerca Scientifica 1, 00133 Rome, Italy*

Sergio Chibbaro and Sauro Succi

*Istituto Applicazioni Calcolo, CNR, V.le del Policlinico 137, 00161, Rome, Italy*

A mesoscopic multi-component lattice Boltzmann model with short-range repulsion between different species and short/mid-ranged attractive/repulsive interactions between like-molecules is introduced. The interplay between these composite interactions gives rise to a rich configurational dynamics of the density field, exhibiting many features of disordered liquid dispersions (micro-emulsions) and soft-glassy materials, such as long-time relaxation due to caging effects, anomalous enhanced viscosity, ageing effects under moderate shear and flow above a critical shear rate.

PACS numbers:

The rheology of flowing soft systems, such as emulsions, foams, gels, slurries, colloidal glasses and related fluids, is a fast-growing sector of modern non-equilibrium thermodynamics, with many applications in material science, chemistry and biology [1]. These materials exhibit a number of distinctive features, such as long-time relaxation, anomalous viscosity, ageing behaviour, whose quantitative description is likely to require profound extensions of non-equilibrium statistical mechanics. The study of these phenomena sets a pressing challenge for computer simulation as well, since characteristic time-lengths of disordered fluids can escalate tens of decades over the molecular time scales. To date, the most credited techniques for computational studies of these complex flowing materials are Molecular Dynamics and Monte Carlo simulations [2]. Molecular dynamics in principle provides a fully ab-initio description of the system, but it is limited to space-time scales significantly shorter than experimental ones. Monte Carlo methods are less affected by these limitations, but they are bound to deal with equilibrium states. As a result, neither MD nor MC can easily take into account the non-equilibrium dynamics of complex flowing materials, such as micro-emulsions, on space-time scales of hydrodynamic interest. In the last decade, a new class of mesoscopic methods, based on minimal lattice formulations of Boltzmann's kinetic equation, have captured significant interest as an efficient alternative to continuum methods based on the discretization of the Navier-Stokes equations for non-ideal fluids [3]. To date, a very popular such mesoscopic technique is the so-called pseudo-potential-Lattice-Boltzmann (LB) method, developed over a decade ago by Shan and Chen (SC) [4]. In the SC method, potential energy interactions are represented through a density-dependent mean-field pseudo-potential,  $\Psi[\rho]$ , and phase separation is achieved by imposing a short-range attraction between the light and dense phases. In this Letter, we provide the first numerical evidence that a suitably extended, two-species, mesoscopic lattice Boltzmann model is capable of reproducing many features of soft-glassy (micro-emulsions), such as structural arrest, anomalous viscosity, cage-effects and ageing under shear. The key feature of our model is the

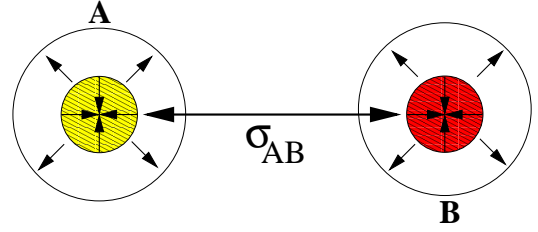


FIG. 1: The two components A and B interact via a repulsive pseudo-potential, which supports a surface tension  $\sigma_{AB}$ . Moreover, each component experiences an attractive interaction in the first Brillouin zone and a repulsive one acting on both Brillouin zones. Each of these interactions can be tuned through a separate coupling constant.

capability to investigate the rheology of these systems on space-time scales of hydrodynamic interest.

The kinetic lattice Boltzmann equation takes the following form [3]:

$$f_{is}(\vec{r}+\vec{c}_i, t+\Delta t) - f_{is}(\vec{r}, t) = -\frac{\Delta t}{\tau_s} [f_{is}(\vec{r}, t) - f_{is}^{(eq)}(\vec{r}, t)] + F_{is} \Delta t \quad (1)$$

where  $f_{is}$  is the probability of finding a particle of species  $s$  at site  $\vec{r}$  and time  $t$ , moving along the  $i$ th lattice direction defined by the discrete speeds  $\vec{c}_i$  with  $i = 0, \dots, b$ . The left hand-side of (1) stands for molecular free-streaming, whereas the right-hand side represents the time relaxation (due to collisions) towards local Maxwellian equilibrium on a time scale  $\tau_s$  and  $F_{is}$  represents the volumetric body force due to inter-molecular (pseudo)-potential interactions. The pseudo-potential force within each species consists of an attractive component, acting only on the first Brillouin region (belt), and a repulsive one acting on both belts, whereas the force between species is short-ranged and repulsive:

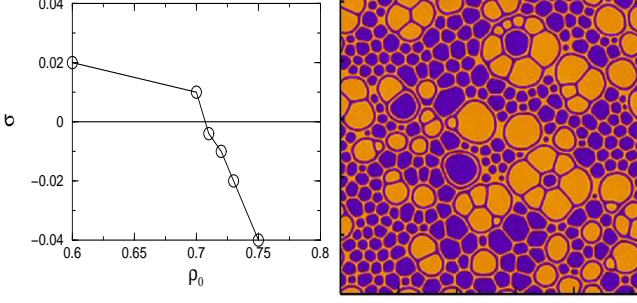


FIG. 2: The nominal surface tension of the two-component fluid as a function of the reference density  $\rho_0$  (left panel). The coupling parameters are  $G_{A1} = -12.55$ ,  $G_{A2} = 11.70$ ,  $G_{B1} = -11.80$ ,  $G_{B2} = 10.95$ ,  $G^X = 0.58$ . By increasing the reference density  $\rho_0$ , the relative strength of interspecies repulsion is weakened as compared to other interactions, thus leading to a net decrease of the surface tension. Above a critical value,  $\rho_{crit} \sim 0.72$ , the nominal surface tension turns negative. Right panel: A typical snapshot of the density field  $\rho_A$  at time  $2 \times 10^6$  (lattice units) at resolution  $512^2$ . Because of the small but positive value of  $\sigma$ , the system proves capable of supporting fairly complex metastable density configurations.

$\vec{F}(\vec{r}, t) = \vec{F}_s^a(\vec{r}, t) + \vec{F}_s^r(\vec{r}, t) + \vec{F}_s^X$ , where

$$\begin{aligned}\vec{F}_s^a(\vec{r}, t) &= G_s^a \Psi_s(\vec{r}; t) \sum_{i=0}^{b_1} w_i \Psi_s(\vec{r}_{1i}, t) \vec{c}_{1i} \Delta t, \\ \vec{F}_s^r(\vec{r}, t) &= G_s^r \Psi_s(\vec{r}; t) \sum_{i=0}^{b_1} p_{1i} \Psi_s(\vec{r}_{1i}, t) \vec{c}_{1i} \Delta t \\ &\quad + G_s^r \Psi_s(\vec{r}; t) \sum_{i=1}^{b_2} p_{2i} \Psi_s(\vec{r}_{2i}, t) \vec{c}_{2i} \Delta t \quad (2) \\ \vec{F}_s^X(\vec{r}; t) &= \frac{G_{AB}}{\rho_0} \rho_s(\vec{r}; t) \sum_{i=0}^{b_1} w_i \rho_{s'}(\vec{r}_i; t) \vec{c}_i \Delta t\end{aligned}$$

In the above, the indices  $k = 1, 2$  refer to the first and second Brillouin zones in the lattice (belts, for simplicity),  $\vec{c}_{ki}$ ,  $p_{ki}$ ,  $w_i$  are the corresponding discrete speeds and associated weights.  $G_{AB} \equiv G_{ss'} = G_{s's}$ ,  $s' \neq s$ , is the cross-coupling between species,  $\rho_0$  a reference density to be defined shortly and, finally,  $\vec{r}_{ki} \equiv \vec{r} + \vec{c}_{ki} \Delta t$  are the displacements along the  $i$ -th direction in the  $k$ -th belt. These interactions are sketched in Figure 1. Note that positive(negative)  $G$  code for repulsion(attraction) respectively. Our model is reminiscent of the potentials used to investigate arrested phase-separation and structural arrest in charged-colloidal systems [6], and also bears similarities to the NNN (next-to-nearest-neighbor) frustrated lattice spin models [7]. As compared with lattice spin models, in our case a high lattice connectivity is required to ensure compliance with macroscopic non-ideal hydrodynamics, particularly the isotropy of potential energy interactions, which lies at the heart of

the complex rheology to be discussed in this work. To this purpose, the first belt is discretized with 9 speeds ( $b_1 = 8$ ), while the second with 16 ( $b_2 = 16$ ) for a total of  $b = 24$  connections. The weights are chosen in such a way as to fulfill the following normalization constraints [8]:  $\sum_{i=0}^{b_1} w_i = \sum_{i=0}^{b_1} p_{i1} + \sum_{i=0}^{b_2} p_{i2} = 1$ ;  $\sum_{i=0}^{b_1} w_i c_i^2 = \sum_{i=0}^{b_1} p_{i1} c_{i1}^2 + \sum_{i=0}^{b_2} p_{i2} c_{i2}^2 = c_s^2$ ,  $c_s^2 = 1/3$  being the lattice sound speed. The pseudo-potential  $\Psi_s(\vec{r})$  is taken in the form first suggested by Shan and Chen [4],  $\Psi_s[\rho] = \sqrt{\rho_0}(1 - e^{-\rho/\rho_0})$ , where  $\rho_0$  marks the density value at which non ideal-effects come into play. Following [9], Taylor expansion of (2) to fourth-order in  $\Delta t$  delivers the non-ideal pressure tensor  $P_{\alpha\beta}(\vec{r}; t)$ , namely

$$P_{\alpha\beta} = [c_s^2 \rho + \frac{1}{2} c_s^2 G_{A1} \Psi_A^2 + G_{B1} \Psi_B^2 + c_s^4 \Pi] \delta_{\alpha\beta} - c_s^4 \gamma_{\alpha\beta} \quad (3)$$

where greek indices run over spatial dimensions and:

$$\begin{aligned}\Pi &= \sum_{s=A,B} G_{s2} [\frac{1}{4} (\nabla \Psi_s)^2 - \frac{1}{2} \Psi_s \Delta \Psi_s] + \\ \frac{G_{AB}}{\rho_0} [\rho_A \Delta \rho_B + \rho_B \Delta \rho_A - \nabla \rho_A \cdot \nabla \rho_B] \quad (4)\end{aligned}$$

$$\begin{aligned}\gamma_{\alpha\beta} &= \sum_{s=A,B} G_{2s} \partial_\alpha \Psi_s \partial_\beta \Psi_s + \\ \frac{G_{AB}}{2\rho_0} (\partial_\alpha \rho_A \cdot \partial_\beta \rho_B + \partial_\alpha \rho_B \cdot \partial_\beta \rho_A) \quad (5)\end{aligned}$$

In the above equations, we have introduced the effective couplings  $G_{s1} = G_s^a + G_s^r$  and  $G_{s2} = G_{s1} + \frac{12}{7} G_{s2}$ ,  $s = A, B$ , respectively. The non ideal pressure splits into a local (bulk) and non-local (surface) contributions, which fix the surface tension  $\sigma$  of the model. It is crucial to appreciate that the value of  $\sigma$  can be tuned by changing the reference density  $\rho_0$ . The repulsive intra-species force  $\vec{F}_s^r$  (proportional to  $\sqrt{\rho_0}$ ) acts against the inter-species repulsive force  $\vec{F}_s^X$  (proportional to  $1/\rho_0$ ). Thus, for small  $\rho_0$ ,  $\vec{F}_s^X$  dominates and a complete separation between the two fluids is expected. This is the case of large and positive  $\sigma$ . On the other hand, for large  $\rho_0$ ,  $\sigma$  becomes smaller and even negative. In figure 2 (left panel), we show  $\sigma$  as a function of the reference density  $\rho_0$ , as obtained through a standard Laplace test on a single bubble configuration. As anticipated, the surface tension decreases at increasing  $\rho_0$  and becomes negative beyond a given threshold,  $\rho_0 > 0.71$ . In this work we shall be concerned only with the case of small and positive  $\sigma$ . In the following, we shall discuss numerical simulations with random initial conditions for the two densities  $\rho_A$  and  $\rho_B$ . After a short transient, the interfacial area reaches its maximum value and progressively tends to decrease due to the effect of surface tension which drives the system towards a minimum-interface configuration. In the long term, this minimum-area tendency would lead to the complete separation between components A and B, with a single interface between two separate bulk components. However, such a tendency is frustrated (hence, strongly retarded) by the complex interplay between repulsive (short-range inter-species and mid-range intra-

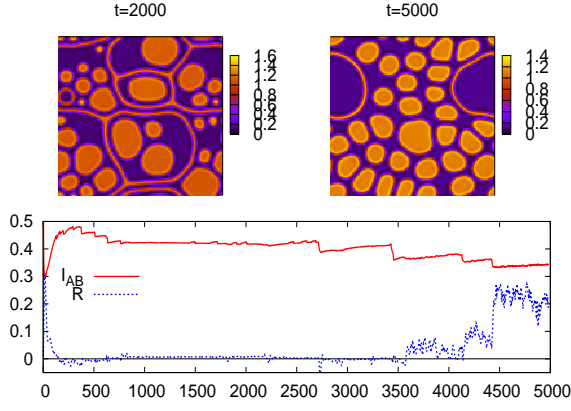


FIG. 3: The response function  $R$  and the surface indicator  $I_{AB}$  as a function of time, (expressed in units of  $10^3$  LB time-steps). The forcing is  $U_0 = 0.1$ , the domain is  $128^2$  and the other parameters are defined in the text. The sharp decrease of the response function in the initial stage indicates the structural arrest of the system, associated with an anomalous enhancement of the flow viscosity, about four orders of magnitude above the molecular value. In the left panel, cages are present, which manage to “trap” micro-structures inside. In the right panel, the cages break down and the system is now able to flow again.

species) and attractive (short-range intra-species) interactions. The final result is a rich configurational dynamics of the density field, as the one shown in figure (2) right panel. In order to investigate the rheological properties of the composite LB fluid, we put the system under a shear flow  $U_x(x, y) = U_0 \sin(ky)$ ,  $U_y = 0$ , and measure the response function  $R = \frac{\bar{U}}{U_0} = \frac{\nu_0}{\bar{\nu}}$ , where  $\bar{U} = \sum_y U(x, y)/N_y$  and  $\bar{\nu}$  defines the effective viscosity. Under normal flow conditions,  $R = 1$ , so that  $R \ll 1$  provides a direct signal of enhanced viscosity and eventually, structural arrest. The main coupling parameters are  $G_A^a = -12.55$   $G_A^r = +11.80$   $G_B^a = -11.70$   $G_B^r = +10.95$   $G_{AB} = +0.58$ , and  $\rho_0 = 0.7$ . These parameters correspond to both species in the dense phase, with no phase transition, hence they can be regarded as descriptive of glassy micro/nanoemulsions, namely a dispersion of liquid within another, immiscible liquid. By letting each species undergo phase transitions between a dense and light phase, the same model could describe foamy materials as well. The simulations are performed mostly on a grid  $128^2$  (except the one reported in figure (2) up to  $5 \times 10^6$  LB time-steps. In figure 3, we show the time evolution of the response  $R$ , as well as an indicator of the interface area,  $I_{AB} = \sum_{x,y} \nabla \rho_A \cdot \nabla \rho_B$ . From this figure, we appreciate a very dramatic drop of the flow speed in the initial stage of the evolution, corresponding to a very substantial enhancement of the fluid viscosity (about four orders). The system remains in this ‘arrested’ state for a very long time, over three millions timesteps, until it suddenly starts to regain its initial velocity through a bumpy dynamics, characterized by a series of sudden jumps [10].

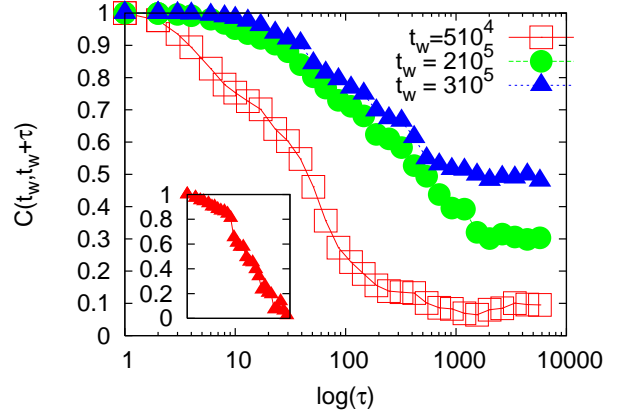


FIG. 4: Ageing of the system. Correlation function corresponding to different waiting times  $t_w$  ( $t_w = 5 \cdot 10^4$ , red squares,  $t_w = 2 \cdot 10^5$ , green circles and  $t_w = 3 \cdot 10^5$ , blue triangles) with shear stress  $U_0 = 0.02$ . In the inset, we show the correlation function for  $t_w = 3 \cdot 10^5$  and  $U_0 = 0.03$ : with increasing shear stress the structural arrest disappears.

These viscosity jumps signal ‘plastic events’, whereby the system manages to break the density locks (cages) which blocked the flow in the initial phase. As a result, the system progressively regains its capability to flow. These plastic events are also recorded by the time trace of the interface area  $I_{AB}$ , which exhibits an alternate sequence of plateaux followed by sudden down-jumps, the latter being responsible for the overall reduction of the interface area as time unfolds. Visual inspection of the fluid morphology confirms this picture. In the top panels of figure 3, we show the density field in an arrested state at time  $t = 2 \cdot 10^5$  (top-left) and in a flowing state,  $t = 5 \cdot 10^5$  (top-right). The left figure clearly reveals the existence of “cages” in the density field configuration, which entrap the fluid inside and consequently block its net macroscopic motion. Inter-domain relaxation can only take place in response to ‘global moves’ of the density field, i.e. the “cage” rupture.

Due to the mesoscopic nature of the present model, the rupture of a single cage in the LB simulation corresponds to a large collection of atomistic ruptures, and consequently it leads to observable effects in terms of structural arrest the system. To the best of our knowledge, this the first time that such an effect is observed by means of a mesoscopic lattice Boltzmann model.

To be noted that the use of high-order lattices (24-speeds) is instrumental to this program, since, by securing the isotropy of lattice tensors up to 8th order, such lattice permits to minimize spurious effects on the non-ideal hydrodynamic forces acting upon the discrete lattice fluid [9]. We next inspect another typical phenomenon of soft-glassy matter, namely ageing. To this purpose, following upon the spin-glass literature [11], we define the order parameter  $\phi \equiv (\rho_A - \rho_B)$  and compute its *overlap*, defined through the autocorrelation of this

order parameter:

$$C(t_w, \tau) = \frac{\langle \sum_{x,y} \phi(x, y; t_w) \phi(x, y; t_w + \tau) \rangle}{\langle \sum_{x,y} \phi(x, y; t_w) \phi(x, y; t_w) \rangle} \quad (6)$$

where  $t_w$  is the waiting time,  $\tau$  is the time lapse between the two density configurations and brackets stand for averaging over an ensemble of realizations. In figure 4, we show the correlation function corresponding to different waiting times  $t_w$  ( $t_w = 5 \cdot 10^4$ , red squares,  $t_w = 2 \cdot 10^5$ , green circles and  $t_w = 3 \cdot 10^5$ , blue triangles) for shear stress  $U_0 = 0.02$ . From this figure, ageing effects are clearly visible, in the form of a slower than exponential decay of the correlation function, which saturates to a non-zero value in the long-time limit (broken ergodicity). In the inset of the same figure, we show the correlation function for  $t_w = 3 \cdot 10^5$  and  $U_0 = 0.03$ : with increasing shear stress the structural arrest disappears, which is one of the most distinctive features of flowing soft-glassy materials [12]. The main advantage of the present lattice mesoscopic approach is to give access to hydrodynamic scales within a very affordable computational budget. With reference to micro-emulsions (say water and oil), we note that the presence of surfactants usually gives rise to microscopic structures of the order of 50 nm in size [14]. These can be likened to the 'blobs' observed in our simulations. With reference to liquid water, we have  $\nu \sim 10^{-6}$  ( $m^2/s$ ), which can be used to obtain a physical measure of the time step  $\Delta t \sim 4$  ps, about three orders of magnitude larger than the typical timestep used in Molecular Dynamics. As a

result, a five-million time-step LB simulation spans about 20 microseconds in physical time. Since the present LB method is easily amenable to parallel computing, parallel implementations will permit to track the time evolution of three-dimensional micro-emulsions of tens of microns in size, over time spans close to the millisecond, i.e. at space-time scales of hydrodynamic relevance. Summarizing, we have provided the first numerical evidence that a two-species mesoscopic lattice Boltzmann model with mid-range repulsion between like-molecules and short-range repulsion between different ones, is capable of reproducing many distinctive features of soft material behaviour, such as slow-relaxation, anomalous enhanced viscosity, caging effects and aging under shear. The present lattice kinetic model caters for this very rich physical picture at a computational cost only marginally exceeding the one for a simple fluid. As a result, it is hoped that it can be used as an alternative/complement to MonteCarlo and/or Molecular Dynamics, for future investigations of the *non-equilibrium* rheology of a broad class of flowing disordered materials, such as microemulsions, foams and slurries, on space and time scales of experimental interest.

SS wishes to acknowledge financial support from the project INFLUS (NMP3-CT-2006-031980). SC wishes to acknowledge financial support from the ERG EU grant and COMETA. Fruitful discussions with L. Biferale, D. Nelson, G. Parisi and F. Toschi are kindly acknowledged. The authors are thankful to A. Cavagna for critical reading of this manuscript.

- 
- [1] W.B. Russel, D.A. Saville, and W.R. Schowalter, *Colloidal Dispersion* (Cambridge University Press, Cambridge England, 1989). P.H. Poole, F. Sciortino, U. Essmann, and H. E. Stanley, *Nature* **360**, 324 (1992). P. Sollich, F. Lequeux, P. Hébraud, and M. E. Cates, *Phys. Rev. Lett.* **78**, 2020 (1997). R.G. Larson, *The structure and Rheology of Complex Fluids* (Oxford University Press, New York, 1999). T. Eckert, and E. Bartsh, *Phys. Rev. Lett.* **89**, 125701 (2002) F. Sciortino, *Nat. Mat.* **1**, 145 (2002). K.N. Pham, et al., *Science* **296**, 104 (2004). H. Guo, et al., *Phys. Rev E* **75**, 041401 (2007). P. Schall, et al., *Science* **318**, 1895 (2007). P. J. Lu, E. Zaccarelli, F. Ciulla, A. B. Schofield, F. Sciortino, and D. A. Weitz, *Nature*, **453**, 499 (2008).
  - [2] M.P. Allen, and D.J. Tildesley *Computer simulations of liquids* (Oxford University Press, New York, 1990). D. Frankel, and B. Smith, *Understanding molecular simulation* (Academic Press, San Diego, 1996). K. Binder, and D.W. Herrman *Monte Carlo simulation in Statistical Physics* (Springer, Berlin, 1997). W. Kob in *Slow relaxation and nonequilibrium dynamics in condensed matter*, eds J.-L. Barrat, M. Feigelman, and J. Kurchan (2002).
  - [3] R. Benzi, S. Succi, and M. Vergassola, *Phys. Rep.* **222**, 145 (1992), S. Chen, and G.D. Doolen, *Annual Rev. Fluid Mech.*, **30**, 329 (1998).
  - [4] X. Shan, and H. Chen *Phys Rev E* **47**, 1815 (1993).
  - [5] G. Falcucci, S. Chibbaro, S. Succi, X. Shan and H. Chen *Eur. Phys. Lett.*, **82** 24005 (2008).
  - [6] F. Sciortino, S. Mossa, E. Zaccarelli, P. Tartaglia. *Phys. Rev. Lett.* **93**, 055701 (2004).
  - [7] J. D. Shore, and J. P. Sethna *Phys. Rev. B* **43**, 3782 (1991)
  - [8] S. Chibbaro, G. Falcucci, X. Shan, H. Chen, and S. Succi, *Phys. Rev. E*, **77**, 036705 (2008).
  - [9] M. Sbragaglia, R. Benzi, L. Biferale, S. Succi, K. Sugiyama, and F. Toschi, *Phys. Rev. E* **75**, 026702 (2007).
  - [10] G.J. Papakonstantopoulos, R.A. Riggelman, J.-L. Barrat, and J. de Pablo, *Phys. Rev. Lett.* **77**, 041502 (2008).
  - [11] G. Biroli, J.-P. Bouchaud, A. Cavagna, T. S. Grigera, P. Verrocchio, *arXiv:0805.4427v1*, (2008).
  - [12] P. Coussot et al., *Phys. Rev. Lett.* **88**, 218301 (2002). L.Buisson, A. Garcimartin, S. Ciliberto, *Europhysics Letters* **63**, 603 (2003)
  - [13] P.G. de Gennes, *Capillarity and wetting Phenomena* (Springer, New York, 2003).
  - [14] S. Wu, H. Westfahl Jr., J. Schmalian, and P. G. Wolynes, *Theory of Microemulsion Glasses*, *Chem. Phys. Lett.* **359**, 1 (2002).